GEOMETRIC CALIBRATION OF ZOOM LENSES
FOR COMPUTER VISION METROLOGY

Dr. Anthony G. Wiley, Major, U.S. Army
U.S. Army Space Programs Office
U.S.A.
Commission V

Dr. Kam W. Wong, Professor of Civil Engineering
University of Illinois at Urbana-Champaign
U.S.A.
Commission V

ABSTRACT:

Zoom lenses are used extensively in computer vision to overcome the limited resolution provided by the small focal planes of solid-state cameras. Laboratory studies of zoom lenses, with a focal range of 12.5-75 mm, showed that geometric distortions could amount to several tens of pixels across the focal plane, and that there were significant changes in the distortion patterns at the different focal settings. Changes in the position of the principal point amounting to as much as 90 pixels were measured. Fortunately, these changes were found to be highly systematic over the entire range of zoom, and were highly repeatable and stable over time. A mathematical model was developed to model the geometric distortions at a fixed focal setting with an RMS error better than $\pm$ 0.1 pixel. A method was devised to model the changes in the interior geometry of zoom lenses, with the resulting residual distortions amounting to less than $\pm$ 0.4 pixel (RMS). Laboratory results demonstrated that three-dimensional positioning using properly calibrated zoom lenses could improve the accuracy as much as 200%.

KEY WORDS: Zoom lenses, geometric calibration, computer vision, metrology.

1. INTRODUCTION

Zoom lenses have not played any significant role in photogrammetric applications. It has been common knowledge that major changes in both the interior geometry and distortion characteristics occur with changes in the focal length setting. Fryer (1986) found that changes in radial distortions of zoom lenses is negligible only for focal settings greater than 50 mm. However, limiting the use of zoom lenses to focal lengths greater than 50 mm effectively nullify much of the advantage of the zooming capability. In one attempt to use zoom lenses in photogrammetric operations, Schwartz (1989) reported on a vision system that provided real-time calibration of the zoom lens whenever the focal length was changed, through the use of a super-imposed reseau grid. Extensive literature search did not find any further quantitative data on the changing distortion characteristics of zoom lenses, nor any report on the use of zoom lenses for accurate photogrammetric measurements.

On the other hand, zoom lenses are being used extensively in machine and robot vision because of the limited resolution capability of video cameras. Typically, the video cameras used in vision application have a focal plane measuring only about 9 mm x 7 mm, resulting in a very small imaging area as compared to conventional film cameras. Zoom lenses are needed to provide the capability to change the focal setting on computer command so that large areal coverage can be obtained at short focal settings while close-up views are achieved at long focal settings.

If geometric fidelity can be maintained on the focal plane for the entire range of zoom, longer focal settings will also result in higher measurement accuracy in the three-dimensional object space. This paper reports on the results of a study that was aimed at developing methodologies to calibrate, model, and correct for geometric distortions in zoom lenses for applications in computer vision metrology. The goal was to evaluate the geometric stability of zoom lenses, and to develop calibration techniques so that increase in 3-D positioning accuracy can be achieved at longer focal settings.

2. VISION EQUIPMENTS

Experimental tests were conducted in the Vision Research Laboratory of the U.S. Army Advanced Construction Technology Research Laboratory at the University of Illinois at Urbana-Champaign. An International Robomation/Intelligence (IRI) DX/VR vision system was used for image capture (Wong et al, 1990).

Available for use in this study were two General TCZ-200 interline-transfer charge-coupled device (CCD) cameras, and two Pulnix TM80 frame-transfer CCD cameras. All four cameras had a focal plane of approximately 8.8 mm x 6.6 mm, which corresponds to an aspect ratio of 4:3 for standard RS170 video signal. The focal plane of the General cameras consisted of 510 horizontal by 490 vertical pixels. Each pixel has an exterior dimension of 0.017 mm(H) x 0.013 mm (V), with only about 30% of the surface area being light sensitive. The focal plane of the Pulnix TM80 cameras consisted of 800(H) x 490(V) pixels, with nearly the entire surface area of each pixel being light sensitive. The effective resolution of the General cameras was 370(H) x 350(V) TV lines, whereas that of the Pulnix cameras was 525(H) x 350(V) TV lines. Two Fujinon 12.5-75 mm, F1.2 and two Computar 12.5-75 mm, F1.8 zoom lenses were made available for this study. Each digital image from the vision system consisted of 512x512 pixels, with the grey level of each pixel represented by an integer number between 0 and 255 resulting in 256 grey levels.

All program development and data processing were performed on two monochrome DN4000 and one color DN3000 Apollo workstations, which were part of an Apollo network that consisted of over 75 terminals.

The high-speed, multi-window, multi-tasking capability of the workstations provided an efficient platform to handle the heavy computation load. Image files were transferred between the IRI DX/VR vision system and the Apollo workstations by means of 5.25-inch floppy disks.

3. CONTROL FIELD

A three-dimensional control field, see Figure 1, was established for zoom lens calibration. It consisted of 54 round, black targets on white background. There were ten targets of 38.1-mm diameter, eight targets of 76.2-mm diameter, and 36 targets of 101.6-mm diameter. Each target was identified through the use of a six-digit binary bar code located beneath the target. A short bar represented
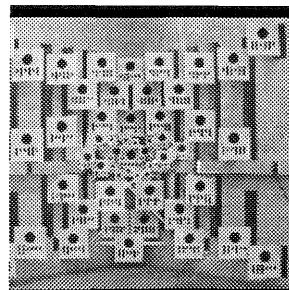
Figure 1. Three-dimensional control field

a zero, and a long bar represented a 1. The entire control field covered an area of 2.25 m(H) x 2.75 m(W) x 2.41 m(D). The locations and sizes of the targets were designed so as to provide a minimum of 12 targets of sufficient size and dispersion to facilitate the calibration of zoom lenses of the entire focal range of 12.5 mm to 75 mm. The three-dimensional coordinates of the center of each target were determined by triangulation. The average estimated standard errors of the target coordinates were computed to be: $\sigma_x = \pm 0.3$ mm, $\sigma_y = \pm 0.8$ mm, and $\sigma_z = 0.4$ mm. The X- and Z- axes lied in a vertical plane, with the X-axis being horizontal and the Z-axis being in the vertical direction. The Y-axis was horizontal and approximately along the depth of the target field.

4. DISTORTION MODEL

After extensive experimental tests, the following model was found to provide excellent representation of the distortion characteristics of a vision system at a given focal length setting(Wiley and Wong, 1990; Wong et al, 1991):

$$dx = l_1\overline{x}r^2 + [p_1(r^2 + 2\overline{x}^2) + 2p_2\overline{xy}]$$

$$dx = l_1\overline{y}r^2 + [2p_1\overline{xy} + p_2(r^2 + 2\overline{y}^2)]$$

$$\overline{x} = (x - x_p)(1 + k)$$

$$\overline{y} = y - y_p$$

$$r^2 = \overline{x}^2 + \overline{y}^2$$

where x and y are image coordinates; x_p and y_p are image coordinates of the principal point; k is a scale factor for the x-coordinates; L_1 is the first term of symmetric radial distortion; and p_1 and p_2 are the first two terms of decentering lens distortions.

5. TARGETING ALGORITHM

An algorithm was developed to automatically identify and locate the center of each target in an image. It consisted of the following steps:

1. find the approximate locations and identification numbers of all the targets in an image using the method reported in Wong et al (1988);
2. perform sub-pixel edge detection along the boundary of each target using local thresholds; and
3. compute the image coordinates of the center of each target by least-squares fitting with an elliptical template.

The estimated standard error of the computed coordinates of the target centers typically ranged between $\pm$ 0.005 and $\pm$ 0.02 pixel. There was no significant difference in the targeting accuracy of the two types of cameras used, in spite of the slightly higher resolution of the Pulnix cameras. This was largely attributed to the size of the targets, which typically had a diameter of more than 10 pixels in the calibration images.

6. CALIBRATION IMAGES

Images of the control field were obtained using the following six different combinations of camera and zoom lenses:

Combination	Camera	Serial No.	Lens	Serial No.
1	Pulnix TM80	001146	Fujinon	987894
2	Pulnix TM80	001136	Computar	1473508
3	General TCZ-200	7001009	Computar	1472638
4	Pulnix TM80	001146	Fujinon	994104
5	Pulnix TM80	001136	Fujinon	994104
6	General TCZ-200	6027001	Computar	1473508

In each case, the camera-lens combination was positioned in front of the control field and at a distance of approximately 5.5 m from the center of the target field. A total of 16 images were acquired in sequence for each combination at the following nominal focal settings: 12.5, 15, 20, 25, 30, 35, 40, 45, 50, 55, 60, 65, 70, 75, 12.5, and 15 mm.

7. FREE CALIBRATION

A free calibration was performed for each focal setting of each camera-lens combination by a bundle adjustment. Only the object-space coordinates of the control targets were constrained in an adjustment, which yielded the following: six exterior orientation parameters of the camera (X^c, Y^c, Z^c, ω, ϕ, and κ); and five interior orientation parameters (f, k, L_1, p_1, and p_2).

Table 1 lists the root-mean-square errors (RMS) of the residuals for all the adjustments. For focal length of 35 mm or shorter, the RMS errors were between $\pm$ 0.05 and $\pm$ 0.09 pixel. The small magnitude of the RMS errors for these adjustment confirmed the validity of the distortion model as well as the accuracy capability of the targeting algorithm. For focal lengths greater than 35 mm, largely because of the fewer number of control points available in each calibration image and the degradation in resection geometry, the RMS errors were increased to between $\pm$ .07 and $\pm$ .17 pixels.

Figure 2 shows the changes in the interior and exterior orientation parameters with respect to the focal setting for camera-lens combination 4. Space limitation does not permit the inclusion of similar plots for the other five cases. As can be expected, there were small systematic changes in the exterior orientation parameters. Changing the focal setting resulted in a small movement of the exposure center and, in some cases, small changes in the direction of the optical axis. In all six cases, the changes in the interior orientation parameters were also highly systematic.

Of particular interest from the free calibration results are that 1) there were large linear shift of the principal point, and 2) decentering distortions were quite large. For camera-lens combinations Nos. 2 and 5, which involved the same camera, linear shift of the principal point amounted to about 90 pixels, and decentering distortions amounted to about 5 pixels near the edge of the images acquired with f= 75 mm. Discussions with A. Burner of NASA led to the conclusion that both of these phenomena were most likely caused by tilting of the optical axis with respect to the focal plane. Burner reported that tilts of up to 0.5 degree were not uncommon in this type of cameras (Burner et al, 1990). A linear shift of the principal point amounting to 80 pixels over the zoom range of 12.5 mm to 75 mm would be equivalent to a tilt of only 1 degree.

One obvious approach to zoom lens calibration is to simply model these patterns with a separate polynomial for each of the parameters. Another possible approach is to use these calibration results directly in a table look-up scheme. The problem with both of these two approaches is that corrections for changes in exterior orientation parameters must be applied for different focal settings.

Further analysis of the results from free calibration showed that the RMS errors for the exterior orientation parameters were quite large comparing to the magnitude of changes when the focal length was varied between 12.5 and 75 mm. Much of the problem was due to the small field of view at
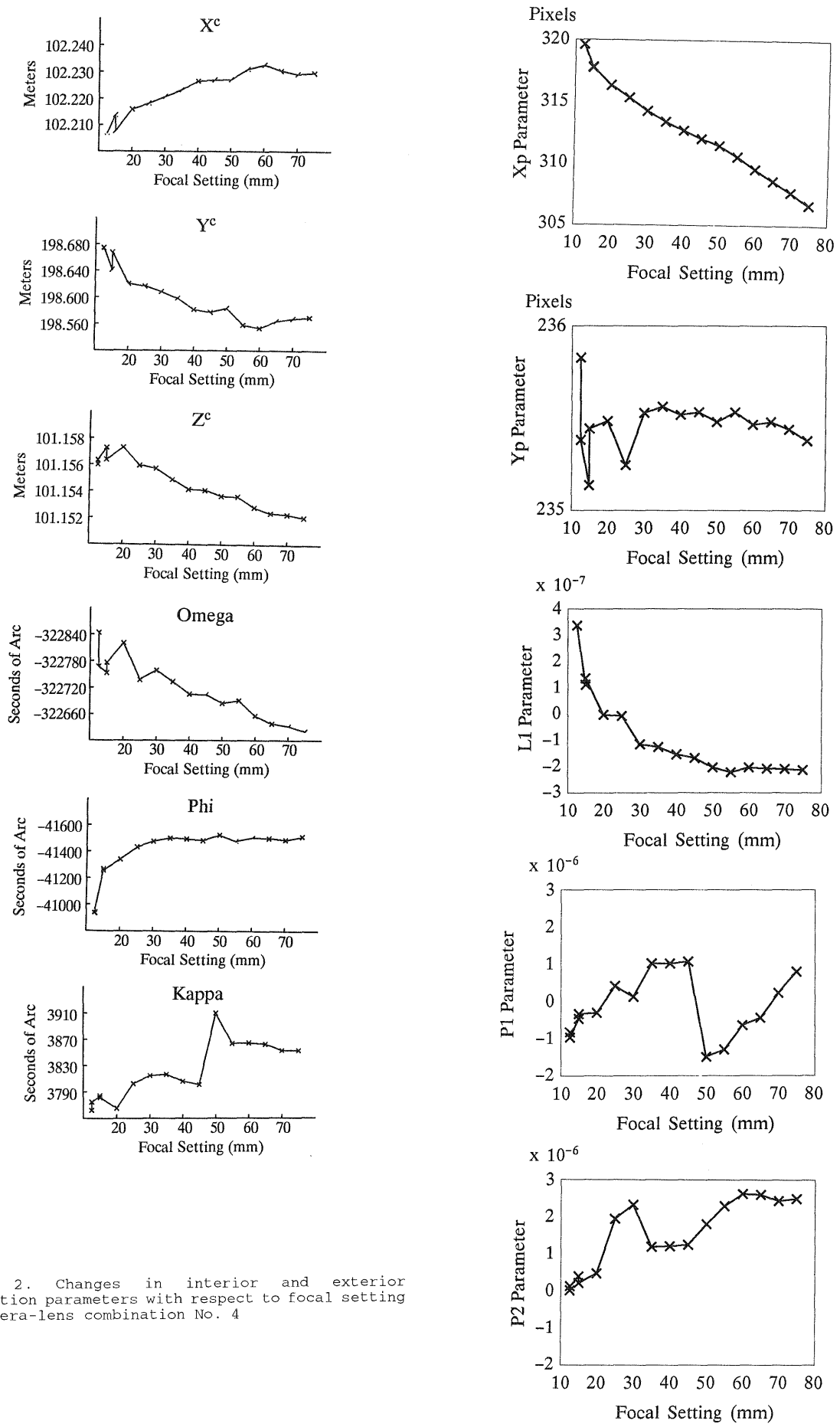
Figure 2. Changes in interior and exterior orientation parameters with respect to focal setting for camera-lens combination No. 4

long focal setting. At a focal length setting of 12.5 mm, the diagonal field of view was 30°. At the focal setting of 50 and 75 mm, the field of view decreased to 8° and 5° respectively. Such narrow field of view resulted in very poor resection geometry for camera calibration. The correlation between the focal length and the distance of the camera from the control field, in this case represented by the coordinate Y^c, also increased significantly with increase in the focal length. For the test cases reported here, the correlation coefficient between the focal length (f) and the coordinate Y^c was -0.02 for f= 15 mm; but increased to -0.6 at f = 55 mm.

8. SEQUENTIALLY CONSTRAINED CALIBRATION

Because of the above observation, it was decided to develop a calibration procedure based on the assumption that all the exterior orientation parameters remained fixed when the focal length was varied. Physically, it could be visualized that the focal plane, instead of the exposure center, actually moved back and forth with changes in the focal length. The assumption facilitated the calibration process, and was not found to be significantly detrimental to the results. Distortions resulted from fixing the exterior orientation parameters were largely absorbed by the interior orientation parameters. Changes in the interior orientation parameters were modeled using first- and second-degree polynomials.

The following procedure of sequentially constrained solution were found to yield very satisfactory results:

1. perform a free calibration independently for each focal setting, and compute the average value of Z^c from this set of results;
2. repeat the calibration solution for each focal setting with the Z^c coordinate fixed, and compute the average value of X^c from the results;
3. repeat the calibration solution for each focal setting with the coordinates Z^c and X^c fixed, and compute the average value of Y^c from the results;
4. repeat this process successfully for the rotation parameters κ, ω, and ϕ;
5. repeat the calibration solution for each focal setting with all six exterior orientation parameters held fixed, and accept the computed effective focal length for each focal setting;
6. repeat the calibration solution only for images obtained at f equal to 12.5 and 15 mm, and compute the average value of k from the results;
7. repeat the calibration solution for each focal setting by holding fixed the six exterior orientation parameters, the focal length f, and the scale factor k; and model the resulting values of x_p and y_p separately with a first-order polynomial;
8. repeat the calibration solution for each focal setting by holding fixed all processed parameters with the values of x_p and y_p computed from the newly developed model; and then model the resulting values of L_1 with two separate second-degree polynomials, one for vales of f equal to or smaller than 25 mm, and one for f equal to or greater than 25 mm; and
9. repeat the calibration solution for each focal setting with only p_1 and p_2 as unknowns; and model the resulting values of p_1 and p_2 with separate second-degree polynomials.

The parameter to be fixed at a given iteration was decided from an analysis of the RMS errors of the computed parameters. The remaining unknown parameters with the smallest RMS error was selected as the next parameter to be fixed.

The resulting distortion models for the interior orientation parameters of the six camera-lens combinations are summarized in Table 2. The effectiveness of the sequential modelling procedure can be evaluated by comparing the RMS errors of the residuals after free calibration in Table 1 with those from the sequential constrained calibration in Table 3. In free calibration, the average RMS error of the residuals was ± 0.07 pixel for f= 12.5 mm and ± 0.15 pixel for f= 75 mm. In sequentially constrained calibration, the average RMS error of the residuals was ± 0.18 pixel for f = 12.5 mm and ± 0.27 pixel for f= 75 mm. The increases in RMS

errors were due to 1) the assumption that the exterior orientation parameters remained fixed throughout the entire range of zoom, and 2) the modelling of the changing patterns of the interior orientation. It is encouraging to note, however, that in all cases of sequentially constrained calibration, the RMS residual errors were less than ± 0.4 pixel.

The potential benefit of calibrated zoom lenses in photogrammetric measurement is also demonstrated by the results in Table 3. As the focal length was changed from 12 mm to 75 mm, the increase in image scale amounted to 500%; while the corresponding increase in RMS image residuals was only between +29% and +84% for the six camera-lens combinations. Thus, an increase in 3-D positioning accuracy will be possible by using longer focal setting, since the increase in image residual errors can be offset by a much larger increase in image scale.

9. STABILITY TESTS

Two tests were conducted to evaluate the stability and repeatability of the distortion patterns. In one test, camera-lens combination 4 was used to collect a second set of images of the control field at the same 16 focal settings as those listed in Tables 3. This set of images were acquired 7 days after the set used for generating the distortion model reported under camera-lends combination 4 in Table 2. The distortion models developed using the first set of images were used to apply corrections to the second set of images. The exterior orientation parameters for the second set of images were computed using images collected at focal settings of 12.5 and 15 mm only. The residuals in the corrected image coordinates were then computed from the known object-space coordinates of the control targets. The RMS errors of these image residuals are listed in Table 4. Table 4 also lists the results from the second test using camera-lens combination 2. In that case, the two sets of images were collected 14 days apart. It can be seen from Table 4 that there were no significant differences in RMS errors for both tests, verifying that distortion patterns of the interior orientation parameters were highly stable and repeatable. These tests clearly demonstrated the feasibility of applying calibration techniques to zoom lenses in computer vision metrology.

10. APPLICATION TESTS

Stereo images of the control field were also obtained to evaluate the potential advantages of zoom lenses in three-dimensional position measurement. Four sets of stereo images were obtained, with each set consisting of stereo images in three focal settings: 15 mm, 45 mm, and 70 mm. Distortion corrections were applied to all computed image coordinates using previously obtained calibration results. The exterior orientation of the two cameras in each set were determined using only the two images obtained at f=15 mm. In all instances, the cameras were assumed to remain fixed as the focal lengths were increased. Object-space coordinates of the targets were then computed by intersection using the corrected image coordinates and the computed exterior orientation parameters. The computed object-space coordinates were then compared with their known values. The results are tabulated in Table 5.

The accuracy of stereo 3-D measurement depends on the stereo intersecting geometry as well as on the accuracy of the image coordinates. The results in Table 5 clearly shows the potential improvement in accuracy with increase in base separation between the two cameras. Within each camera configuration, significant improvement in accuracy amounting to 200% for configuration 3 and 100% for the other three, was achieved with longer focal length. In fact, at the focal setting of 75 mm, camera configurations 3 and 4 yielded 3-D positioning accuracy approaching that of the control field.

11. CONCLUSIONS

Experiments with six camera-lens combination showed that geometric distortions could amount to several tens of pixels in an image consisting of 512x512

590

pixels, and that there were significant changes in the distortion characteristics with changes in the focal setting. However, the pattern of change for a given camera-lens combination was very systematic and stable over time. Free calibration of individual frames resulted in a residual RMS errors between ± 0.05 and ± 0.1 pixels for f ≤ 35 mm, and between ± 0.05 and ± 0.17 pixel for f > 35 mm.

From an application standpoint, it is more convenient to assume that the exposure center and the optical axis of a zoom lens remain fixed as the focal length is varied. A method of zoom lens calibration was developed based on this assumption. Results showed that this method of sequentially constrained calibration resulted in residual RMS errors of less than ± 0.4 pixel, and improvement of 3-D positioning accuracy by as much as 200%.

The results of this study clearly shows that the geometric calibration of vision systems equipped with 12.5-75 mm zoom lenses is indeed possible. Significant changes in the interior geometry of zoom lenses occur with variation in the focal length. However, a method has been developed to perform zoom lens system calibration. Zoom lenses provide a means of bridging the gap between short and long focal length lenses for photogrammetric applications. They offer the ability to have both the global view of smaller scale imagery as well as the precise metrology and target positioning of large scale imagery. The ability to calibrate CCD camera systems equipped with zoom lenses can open doors to a wide variety of applications heretofore closed.

12. ACKNOWLEDGEMENT

13. REFERENCES

Burner, A.W.; W.L. Snow; M.R. Shortis; and W.K. Goad; (1990) Laboratory Calibration and Characterization of Video Cameras. Proceedings of ISPRS Symposium on Close-Range Photogrammetry Meets Machine Vision (Zurich, Sept. 3-7), SPIE Proceedings, Vol. 1395, pp.664-671.

Fryer, J. G. 1986. Distortion in Zoom Lenses. Australian Journal of Geodesy, Photogrammetry, and Surveying, No. 44, pp. 49-59.

Schwartz, D. S. 1989. Vision Metrology System: An Automated Noncontact Three-Dimensional Measurement System. Technical Papers 1989 ASPRS/ACSM Annual Convention, Vol. 1, Baltimore, MD, pp. 145-156.

Wiley, A.G. and K. W. Wong; 1990. Metric Aspects of Zoom Vision. Proceedings of ISPRS Symposium on Close-Range Photogrammetry Meets Machine Vision (Zurich, Sept. 3-7), SPIE Proceedings, Vol. 1395, pp.112-118.

Wiley, A. G. 1991. Metric Aspects of Zoo Vision. Ph.D. dissertation, University of Illinois at Urbana-Champaign, 1991.

Wong, K.W.; Y. Ke; M. Lew; and M. T. Obaidat; 1991. Three-Dimensional Gaging with Stereo Computer Vision. SPIE Proceedings, Vol. 1526, pp. 17-26.

Wong, K. W.; M. Lew; and Y. Ke; 1990. Experience with Two Vision Systems. Proceedings of ISPRS Symposium on Close-Range Photogrammetry Meets Machine Vision (Zurich, Sept. 3-7), SPIE Proceedings, Vol. 1395, pp. 3-7.

Table 1. Root-Mean-Square Errors of the Residuals After Free Calibration

Focal Setting (mm)	Number of Targets	1	2	Camera-Lens Combination 3 (± pixels)	4	5	6
12.5	38	.07	.05	.09	.06	.05	.07
12.5	38	.06	.05	.09	.05	.06	.06
15	32	.10	.06	.10	.07	.06	.07
15	32	.09	.06	.10	.07	.06	.07
20	25	.08	.06	.08	.07	.06	.07
25	30	.07	.06	.08	.05	.06	.08
30	21	.07	.07	.09	.05	.06	.07
35	20	.07	.08	.09	.05	.07	.08
40	18	.07	.08	.11	.05	.09	.08
45	15	.08	.10	.09	.05	.11	.09
50	13	.10	.10	.11	.06	.09	.09
55	13	.11	.11	.13	.07	.12	.10
60	13	.12	.13	.13	.08	.11	.11
65	13	.15	.14	.14	.10	.12	.12
70	13	.14	.16	.15	.10	.13	.12
75	13	.14	.17	.17	.11	.15	.13

Table 2. Distortion Models for interior Orientation Parameters

Parameter (coeff.)		1	2	Camera-Lens Combination 3	4	5	6
k		0.009	0.0088	0.0327	0.0090	0.0088	0.0330
x_p	a	319.916	331.614	206.682	319.430	262.077	203.814
	b	0.00344	-0.01356	-0.00011	-0.00223	-0.00613	0.00760
y_p	c	237.394	222.822	275.680	235.426	261.160	292.168
	d	-0.00313	-0.01101	0.00644	-2.677E-6	-0.01608	0.00126
L_1	e	2.119E-6	1.548E-6	1.875E-6	1.957E-6	1.698E-6	1.998E-6
	g	-2.615E-9	-1.830E-9	-2.185E-9	-2.303E-9	-2.028E-9	-2.376E-9
	h	7.760E-13	4.812E-13	5.763E-13	6.459E-13	5.449E-13	6.507E-13
	i	2.514E-8	5.722E-8	-2.104E-7	1.234E-7	-3.189E-8	-4.414E-8
	j	-6.849E-11	-1.424E-10	-2.703E-12	-1.380E-10	-1.145E-10	-8.793E-11
	k	4.528E-15	1.359E-14	-2.097E-15	1.392E-14	1.237E-14	1.064E-14
p_1	m	-6.355E-6	-1.979E-6	-5.540E-6	1.367E-6	-2.616E-6	-1.018E-6
	n	4.268E-9	6.119E-9	3.344E-9	-1.221E-9	3.818E-9	-3.971E-9
	s	-8.187E-13	-2.562E-13	-4.404E-13	1.986E-13	-2.990E-13	1.699E-13
p_2	t	8.324E-7	-2.041E-6	1.421E-6	-1.304E-6	-5.261E-6	8.172E-7
	u	4.037E-12	5.031E-9	-3.557E-9	1.554E-9	7.163E-9	-7.265E-10
	v	-1.253E-13	-5.148E-14	2.136E-13	-1.553E-13	-2.439E-13	6.198E-14

where   f = focal length in pixels
$x_p = a + b\ f$
$x_p = c + d\ f$
$L_1 = e + g\ f + h\ f^2$ for $f \le 25$ mm
$L_1 = i + j\ f + k\ f^2$ for $f \ge 25$ mm
$p_1 = m + n\ f + s\ f^2$
$p_2 = t + u\ f + v\ f^2$

Table 3. Root-Mean-Square Errors of the Residuals After Sequentially Constrained Calibration

Focal Setting (mm)	Number of Targets	1	2	Camera-Lens Combination 3 (± pixels)	4	5	6
12.5	38	.15	.22	.21	.14	.19	.18
12.5	38	.15	.22	.20	.15	.19	.18
15	32	.27	.23	.21	.20	.23	.18
15	32	.23	.24	.21	.15	.24	.19
20	25	.15	.20	.15	.14	.17	.19
25	30	.10	.20	.16	.09	.22	.25
30	21	.16	.23	.17	.08	.21	.24
35	20	.10	.21	.16	.09	.28	.26
40	18	.10	.23	.18	.10	.25	.24
45	15	.12	.24	.18	.11	.26	.21
50	13	.14	.28	.26	.12	.27	.20
55	13	.15	.28	.17	.13	.30	.17
60	13	.17	.29	.23	.14	.30	.26
65	13	.19	.31	.25	.15	.34	.27
70	13	.18	.32	.23	.16	.31	.25
75	13	.22	.34	.27	.18	.35	.28
Total change in RMS errors between f= 12.5 mm and 75 mm		+47%	+55%	+35%	+29%	+84%	+56%
Total change in image scale between f= 12.5 mm and 75 mm		+500%	+500%	+500%	+500%	+500%	+500%

Table 4. Stability and Repeatability of Calibration Parameters Over Time

Focal Length (mm)	Number of Targets	RMS Errors of Image Residuals ($\pm$ pixel)			
		Camera-Lens Comb. 4		Camera-Lens Comb. 2	
		Initial Set	7-days Later	Initial Set	14-days Later
12.5	38	.14	.15	.22	.20
12.5	38	.15	.14	.22	.23
15	32	.20	.16	.23	.26
15	32	.15	.15	.24	.24
20	25	.13	.20	.20	.22
25	30	.09	.15	.20	.25
30	21	.08	.14	.23	.23
35	20	.09	.15	.21	.25
40	18	.10	.12	.23	.25
45	15	.11	.16	.24	.27
50	13	.12	.14	.28	.28
55	13	.13	.16	.28	.29
60	13	.14	.19	.29	.31
65	13	.15	.21	.31	.34
70	13	.16	.21	.32	.34
75	13	.18	.21	.34	.35

Table 5. 3-D Positioning Accuracy with Different Focal Length

Camera Config.	Focal Length (mm)	Number of Check Points	Average Target Distance (meters)	Camera Base Distance (meters)	ΔX	RMS Error ΔY ($\pm$ mm)	ΔZ	Relative[*] Accuracy
1	15	27	5.9	0.61	0.62	3.14	0.67	1/1800
	45	14			0.27	1.70	0.18	1/3400
	70	12			0.25	1.61	0.18	1/3600
2	15	28	5.7	0.63	0.75	2.75	0.61	1/2000
	45	14			0.20	1.26	0.18	1/4400
	70	12			0.20	1.25	0.18	1/4500
3	15	30	5.6	1.02	0.87	2.79	0.40	1/1900
	45	15			0.23	1.16	0.17	1/4700
	70	12			0.21	0.90	0.17	1/6000
4	15	33	5.4	1.12	0.66	1.06	0.63	1/3900
	45	15			0.30	1.12	0.17	1/4600
	70	12			0.18	0.52	0.21	1/9200

$$* \quad Relative\ Accuracy = \frac{1}{\left(\dfrac{AverageTargetDistance}{\sqrt{\Delta X^2 + \Delta Y^2 + \Delta Z^2}} \right)}$$